AIAA JOURNAL
Vol. 37, No. 6, June 1999

Numerical Simulation of Laser-Induced Fluorescence Imaging in Shock-Layer Flows

P. M. Danehy* and P. C. Palma†
Australian National University, Canberra, ACT 0200, Australia
R. R. Boyce‡
University of Queensland, Brisbane, Queensland 4072, Australia
and
A. F. P. Houwing§
Australian National University, Canberra, ACT 0200, Australia

Planar laser-induced fluorescence (PLIF) images of nitric oxide in hypersonic flow over a wedge and a hemisphere are compared with a theoretical PLIF model. The theoretical PLIF images are based on computational fluid dynamics (CFD) models including a perfect-gas model and a nonequilibrium chemistry model. Two-dimensional maps of the flow parameters generated by the CFD are used to predict the theoretical PLIF images, including the effects of collisional quenching. We find good agreement between the model and the experimental measurements. We explain how this method of computational flow imaging can be useful for designing experiments.

I. Introduction

AEROSPACE vehicles leaving and entering Earth's atmosphere experience Mach numbers on the order of 25 and stagnation temperatures on the order of 7000 K. Arguably, ground-based facilities offer the only practical means of testing aerospace vehicles during their development. Free-piston shock tunnels are hypersonic-flow facilities designed to simulate these high-speed flight conditions. Measurements obtained in these facilities are used to understand the fluid mechanics and chemistry of hypersonic flows and their effects on space vehicles. The data are commonly used to validate computational fluid dynamics (CFD) codes.[1,2] The validated codes provide a means for predicting in-flight behavior and aid in vehicle design and performance evaluation.

Planar laser-induced fluorescence (PLIF) is a versatile tool for nonintrusively measuring a wide range of flow parameters in supersonic and hypersonic flows.[3] Nitric oxide (NO) is one of the primary spectroscopic species for diagnostics measurements using PLIF. NO is a particularly convenient target species for PLIF in free-piston shock tunnels because large quantities (up to 8% by volume) of NO are naturally produced by the tunnel.

Free-piston shock tunnels present a challenging environment for PLIF. The high-enthalpy flows produced in these facilities cause experimental problems not usually encountered in other flow facilities. There are large pressure and temperature variations that can cause large fluorescence signal variations due to sharp gradients in species densities, Boltzmann fractions, and collisional quench rates, and to changes to the spectral overlap between the laser and the absorption transition. Other problems include laser-beam attenuation and spectral hole burning, spectral interference from other flow species, e.g., O_2, and fluorescence trapping. PLIF has previously been performed in free-piston shock tunnels,[4,5] where quantitative measurements were limited to lower enthalpy flows because luminosity from contaminants in the flow overwhelmed PLIF intensities at higher enthalpy conditions.

In most reactive environments (including supersonic airflows), PLIF signal intensities are complicated by collisional relaxation of the laser-excited molecules, or collisional quenching. In the limit that the collisional quenching rate Q is large compared to that of spontaneous emission A the observed fluorescence intensity is proportional to the species concentration n_{NO} divided by Q. Because Q depends on unknown environmental variables, such as the temperature, pressure, and the gas composition, it is difficult to relate LIF intensities directly to species number density.

In this paper, we apply the quenching and fluorescence models described by Paul et al.[6] to calculate theoretical PLIF images, known as computational flow imaging (CFI) PLIF.[7] Collisional quenching depends on the flow conditions; we determine these flow conditions, including maps of each individual species, from CFD models. The collisional quenching rate is then calculated at each position in the image. Together with information about the exciting laser, we calculate theoretical PLIF images to compare with experimental images.

Theoretical PLIF images are useful for several reasons. Performed prior to an experiment, they can be helpful for designing optimal excitation and detection strategies.[6] For example, the images are useful for choosing rotational transitions that would yield signal intensities within the dynamic range of the detection system. Another important use for the theoretical images is for determining the relative importance of different theoretical (or experimental) parameters and assumptions.

Finally, the potential exists for validation of CFD predictions by direct comparison of CFI-PLIF images with experiments. Such comparisons are particularly useful when PLIF is not able to measure a more fundamental physical parameter, such as temperature. This is frequently the case, especially in turbulent and/or very high-pressure environments. In such cases, CFI-PLIF can provide the best possible point of comparison between experiment and theory.

II. Theory

A. Fluid Mechanics

Because the collisional quenching rate depends on the composition, pressure, and temperature of the flow, calculation of theoretical LIF intensities depends on calculation of the fluid mechanical environment. For this study, we have chosen two simple flow configurations: a wedge and a hemisphere in a hypersonic flow. The wedge is a good test for the theoretical model because it has uniform flow in the postshock region and it generates a Prandtl–Meyer expansion fan at the end of the body. Both of these features provide simple but important tests for the CFI-PLIF.

Flow over a hemisphere provides a more rigorous test for the CFI-PLIF method because it has a much larger range of conditions

Received Jan. 24, 1998; revision received Dec. 10, 1998; accepted for publication Dec. 17, 1998.

*Lecturer, Aerophysics and Laser-Based Diagnostics Research Laboratories, Department of Physics, The Faculties.
†Postdoctoral Researcher, Aerophysics and Laser-Based Diagnostics Research Laboratories, Department of Physics, The Faculties.
‡Research Fellow, Department of Mechanical Engineering.
§Senior Lecturer, Aerophysics and Laser-Based Diagnostics Research Laboratories, Department of Physics, The Faculties.

in a single image. As the gas passes through the bow shock, the pressure jumps by nearly a factor of 60. Then, as it expands around the body, the pressure drops by a factor of 15. The severe range of quench rates, temperature, and other properties is a good test for the CFI-PLIF model. Furthermore, studying a hemisphere flow demonstrates PLIF's capability to perform measurements in three-dimensional flows.

1. Freestream Conditions

The freestream conditions have been determined using a one-dimensional nonequilibrium nozzle flow code STUBE,[8] together with an experimental pitot probe survey. The pitot surveys were used mainly to account for boundary layers that form along the walls of the nozzle. For these conditions, the chemical composition freezes out at some distance downstream of the nozzle throat. We have modified STUBE to allow calculation of sudden vibrational freezing. The frozen vibrational temperature $T_{v,f}$ for each of the molecular species was determined with STUBE. For each species, vibrational relaxation length L_v was calculated at each point along the nozzle centerline using the Landau–Teller model, and was compared with the distance L_f the flow moves for the vibrational energy to fall to $1/e$ of its local value. Sudden freezing occurs when the condition $L_v \ll L_f$ changes rapidly to $L_v \gg L_f$, with the $L_v = L_f$ point defining $T_{v,\infty}$. For the flow condition used in this experiment, we determined $T_{v,\infty}$ to be 2100, 2800, and 1520 K for N_2, O_2, and NO, respectively. When determining the flow conditions downstream of a particular species' vibrational-freezing point, the contribution of the vibrational modes to the energy of the molecular species was fixed at its frozen value.

Despite this method being the preferred way of predicting the freestream conditions, for the hemisphere computation to be discussed we did not invoke vibrational freezing in the one-dimensional nozzle-flow code because the two-dimensional CFD code used to compute this flow ignores vibrational nonequilibrium. Had we invoked vibrational freezing, the total thermal energy input to the CFD code would have been incorrect. The main implication of ignoring vibrational freezing is that the calculated freestream temperature is higher than the actual freestream temperature as described in Sec. III.

2. Wedge CFD

The wedge used in these experiments was a 35-deg half-angle wedge oriented at zero angle of attack in the flow. The wedge had a triangular cross section with a length (along the centerline) of 35.7 mm and a base of 50 mm. Experimentally, we observed that the flow near the shoulder of the wedge separated in a direction nearly parallel to the freestream. Therefore, we have chosen to model this flow theoretically assuming a wedge with a flat section attached to the shoulder as shown in Fig. 1.

The flow in the freestream (region 1) is uniform. An oblique shock forms at the tip of the wedge, resulting in a small uniform-flow region where the gas travels parallel to the surface of the wedge (region 2). At the shoulder of the wedge, a Prandtl–Meyer expansion (region 3) cools the flow and turns it parallel to the top surface of the wedge. At the end of the expansion fan, the gas reaches another uniform region (region 4).

For the wedge experiments, the attached oblique shock wave was weak enough that a perfect-gas treatment of the fluid mechanics is justified. For this condition, we have calculated that both chemistry and vibration are essentially frozen, so that the ratio of the specific heats γ can be taken as 1.4 (Ref. 9). Temperature T_1, pressure P_1, Mach number M_1, and the species concentrations are determined from STUBE. The flow conditions across the oblique shock were determined from the normal shock equation, using the component of the flow velocity normal to shock wave. Given P_2, T_2, M_2, and the flow direction, we calculated the flow through the Prandtl–Meyer expansion fan using the method of characteristics.[10] Finally, the uniform conditions in region 4 were determined from the terminating characteristic of the expansion fan.

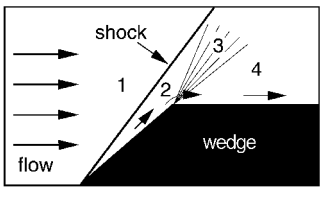

Fig. 1 Definition of flow regions: 1, uniform freestream; 2, postshock region; 3, expansion fan; and 4, postexpansion fan region.

3. Hemisphere CFD

The hemisphere used in these experiments had a 25.4-mm radius. The freestream conditions were identical to those used for the wedge measurement. In the experiment, the flow in the freestream is chemically and vibrationally frozen as described earlier. The flow at the stagnation point at the nose of the hemisphere is in chemical and vibrational equilibrium. As the flow expands around the model it transits regions of chemical and vibrational nonequilibrium and eventually freezes, chemically and vibrationally. Because we did not have access to a CFD code that included both chemical and vibrational nonequilibrium, we were required to make several simplifying assumptions regarding vibrational nonequilibrium: First, the freestream conditions for the hemisphere were calculated assuming vibrational equilibrium. Second, flow over the hemisphere was calculated by using the CFD code of Mundt.[11] This inviscid computation was two-dimensional axisymmetric and included nonequilibrium chemistry, but assumed vibrational equilibrium everywhere. Section IV.C further discusses the impact of the assumptions about the vibrational state of the gas. The CFD code is designed to include boundary-layer computations near the body surface, but this option was not invoked in these calculations.

B. PLIF Theory

The theory of PLIF is well developed.[12] However, only recently has a complete and reliable model[6] been developed that predicts the collisional quenching of nitric oxide by gases relevant to high-temperature, hypersonic airflows. Assuming negligible saturation of the molecular transition and rapid repopulation of the laser-excited ground state, the fluorescence intensity I_{LIF} is[6]

$$I_{\mathrm{LIF}} \propto \phi n_{\mathrm{NO}} \sum_i f_{Bi} B_i g_i \tag{1}$$

where the summation is performed over all transitions i, $\phi = A/(A+Q)$ is the fluorescence yield, f_{Bi} is the Boltzmann fraction, B_i is the Einstein B coefficient, and g_i is the spectral overlap integral

$$g_i = \int_0^\infty g_L g_a \, \mathrm{d}\nu \tag{2}$$

where g_L is the spectral profile of the laser, g_a is the absorption line shape, and both g_L and g_a are normalized so that their integrals over all frequencies equal unity. The laser profile can be specified as either Gaussian or Lorentzian, while the absorption profile can be specified as either Gaussian (for computational efficiency) or Voigt. In these computations, we assumed a Lorentzian laser profile and a Voigt profile for the molecular absorption. The overlap integral also takes into account contributions from nearby transitions; although in this experiment we chose relatively isolated transitions (less than 3% contribution to the signal from nearby lines).

To improve the agreement between theory and experiment, we found that we also needed to account for several other effects not included in the simple model just described. These include saturation of the molecular transitions, laser-sheet attenuation due to absorption, and the intensified charge-coupled device (ICCD) camera's gating time.

Saturation of the molecular transitions was incorporated into the model by multiplying Eq. (1) by the factor

$$\frac{1}{(1 + I/I_{\mathrm{sat}})} \tag{3}$$

where[13]

$$I_{\mathrm{sat}} = h\omega\Gamma_0/\sigma \tag{4}$$

Here the transition cross section σ is evaluated using the Voigt line-shape profile assuming a monochromatic laser. Thus, σ is independent of pressure when Doppler broadening dominates and inversely proportional to pressure when collisional broadening dominates.

Because the population decay rate Γ_0 is proportional to the pressure P (Ref. 14), I_{sat} scales as P^2 in the collisionally broadened limit and as P in the Doppler-broadened limit. Note that in the collisionally broadened limit, this expression is equivalent to those given in Eckbreth[15] and Boyd.[16] Whereas more sophisticated models for saturation exist,[15] this simplified model provides a computationally efficient first-order prediction of saturation. This simplified approach is justified in the present work where saturation has been minimized by keeping the laser intensities low.

The magnitude of the saturation intensity in this work was determined from measurements by Danehy et al.,[14] who measured I_{sat} for the $^{O}P_{12}(1.5)$ transition of nitric oxide in a room-temperature, low-pressure gas cell. Then Eq. (4) was used to scale I_{sat} with respect to temperature, pressure, and line strength. In the experiment, we minimized saturation effects by keeping the laser intensity as low as possible. For the wedge experiments, $I/I_{sat} < 0.15$, whereas in the hemisphere experiments $I/I_{sat} < 0.3$ everywhere except in the freestream, where $I/I_{sat} \approx 0.6$.

Attenuation of the incident sheet of laser radiation due to absorption by the nitric oxide has been modeled using the Beer–Lambert law.[15] At each pixel in the computed image, the absorption coefficient was determined for the range of frequencies contained within the laser spectrum. Assuming that the medium was optically thin across a single pixel, the incoming light was attenuated according to the calculated absorption coefficient and an attenuated spectral laser profile was computed. This modified spectral profile was used in the calculation of the overlap integral g_i to determine the PLIF intensity. This process continued through the entire image. We designed the experiment so that attenuation was minimized to less than about 5% across the imaged flowfield.

Because the fluorescence lifetimes (3–150 ns) in this experiment were comparable to the intensified CCD camera gating times (50–600 ns), the camera attenuated the fluorescence under some experimental conditions. As a first-order correction to account for this effect, we applied a multiplicative correction to Eq. (1) to account for this reduction in PLIF signal. We assumed that the laser pulse length is short compared to the fluorescence lifetime and then determined the fraction F of the exponentially decaying fluorescence collected by the camera:

$$F = 1 - e^{-\tau_{gate}/\tau_{LIF}} \tag{5}$$

where τ_{gate} is the duration of the intensifier gate and $\tau_{LIF} = 1/(A + Q)$ is the fluorescence lifetime. For the wedge experiments described subsequently, $\tau_{gate} = 600 \pm 30$ ns, so that $F \approx 1$. For the case of the hemisphere, F decreases to about one-third in the freestream, where $\tau_{gate} = 50 \pm 30$ ns is smaller than τ_{LIF}.

Effects ignored by the theoretical PLIF model include radiative trapping, transient multilevel population transfer effects, and mode-structure variations in the excitation laser. However, we have designed our experiment to minimize influence of these effects. Radiative trapping was avoided by collecting fluorescence only from transitions terminating in excited vibrational states in the ground electronic state. Multilevel population transfer effects were minimized by keeping the laser intensity low. Finally, the effects of laser mode fluctuations were reduced by signal averaging where possible. No attempt has been made here to determine absolute experimental fluorescence intensities. Thus, all comparisons between experiment and theory shown subsequently have been arbitrarily scaled for best fit.

III. Experiment

The experiments were performed on the T2 free-piston shock tunnel at the Australian National University. A description of the shock tunnel and its operation is given by Stalker.[17] The T2 nozzle has a 15-deg full-angle conical geometry with a 6.4-mm-diam throat and an exit-to-throat area ratio of 144. The test gas in the shock tube was initially 98.9% N_2 and 1.1% O_2 resulting in 98.1% N_2, 1.1% NO, 0.4% O_2, and 0.3% O in the test section during operation. The primary shock speed was 2.4 km/s, which corresponds to a flow enthalpy of 5.8 MJ/kg. The nozzle-reservoir pressure was measured to be 27.0 MPa, and the calculated reservoir temperature was 4500 K (calculated using the equilibrium shock tube code ESTC[18]). The freestream temperature, pressure, Mach number, and velocity calculated assuming vibrational equilibrium were 560 K, 5.6 kPa, 6.6, and 3.2 km/s, respectively (calculated using the quasi-one-dimensional nonequilibrium nozzle-flow code STUBE[8]). The freestream temperature, pressure, Mach number, and velocity calculated assuming sudden vibrational freezing in the nozzle (see Sec. II.A.1) flow were 440 K, 4.5 kPa, 7.7, and 3.2 km/s, respectively.

A schematic of the experiment is shown in Fig. 2. We frequency doubled the output of an excimer-pumped dye laser to obtain 5-mJ light between 224 and 247 nm; this frequency range coincides with the (0, 0), (0, 1), and (0, 2) vibrational bands for the $A^2\Sigma^+ \leftarrow X^2\Pi$ electronic transition of NO. A small portion of the beam was split off and used for wavelength calibration by performing LIF in an H_2/O_2 flame. The laser linewidth was measured to be 0.18 cm^{-1} based on LIF measurements in a gas cell filled with a low pressure of nitric oxide. This is consistent with specifications from the manufacturer.

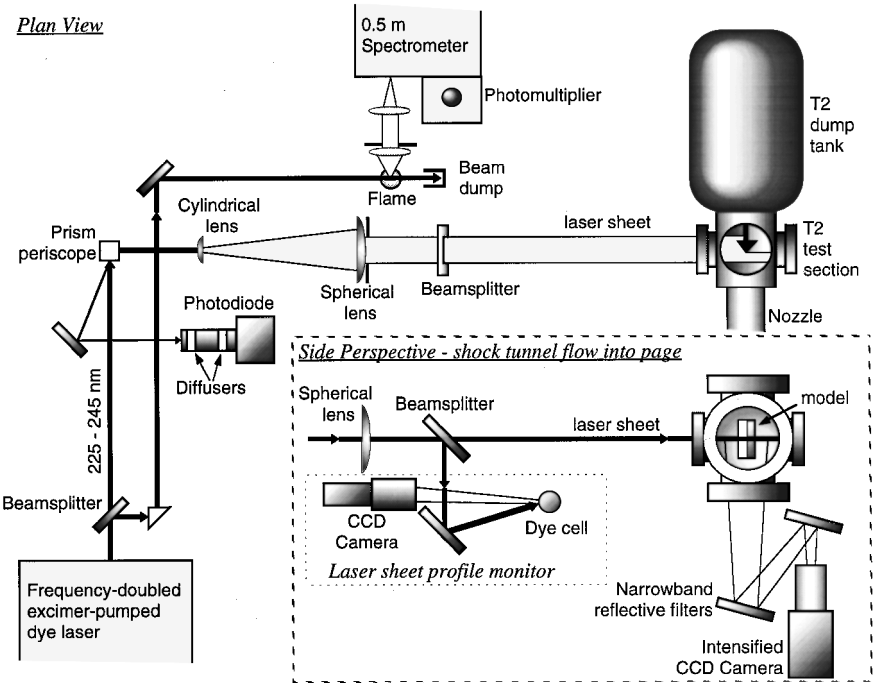

Fig. 2 Arrangement of apparatus for PLIF experiments on the T2 shock tunnel.

We tuned the laser to a NO transition prior to each experimental run of the shock tunnel. Immediately before the run (<2 s), the tunnel operator stopped the laser via a remote switch next to the firing valve. After the firing valve was opened, the nozzle-reservoir pressure transducer detected the shock reflection at the end of the shock tube and the laser was fired 350 μs later. This delay was chosen to coincide with the period of steady flow in the shock tube. An ICCD camera (in-house assembled dual-MCP, fiber optically coupled to an 8-bit CCD, 512 × 240 pixels, ≥50-ns gating period) captured the fluorescence image at right angles to the laser sheet. The fluorescence was reflected off two dielectric mirrors that only directed the nonresonant fluorescence bands $v'' = 2$, 3, and 4 toward the camera.[19] This transmission function was chosen to maximize the signal while minimizing natural flow luminosity and reducing influences from radiative trapping.

The variation in energy across the laser sheet was measured simultaneously with a dye cell and CCD camera.[20] This energy distribution measurement was then used to correct the PLIF image, and it also accounts for pulse-to-pulse spatial fluctuations in the laser energy.

The spectrum of the laser also fluctuated because of mode competition within the laser cavity. These spectral fluctuations lead to uncertainties in the measured PLIF intensities, especially in the lower temperature and pressure regions of the flow where the absorption transitions are narrower and smaller than the laser linewidth. In higher pressure regions of the flow, the uncertainties caused by mode fluctuations are significantly reduced because of the increased broadening of the transitions. The uncertainty due to laser mode fluctuations has been reduced in the wedge experiments by averaging repeated images.

IV. Results

A. Simulated PLIF Image

Investigating the computation of an individual PLIF image can be informative because contributions to the signal intensity from different terms in Eq. (1) can be identified. Figures 3 and 4 show the computation of a PLIF image for the wedge flow assuming the laser is tuned to the $^{R}R_{22}(26.5)$ transition of NO at 44441.1 cm^{-1}, and the laser has a linewidth of 0.18 cm^{-1}. The wedge is shown in the bottom right-hand corner of Figs. 3a–3e. Flow is from left to right. Each image is 50 × 50 mm. The fluorescence intensity (Fig. 3e) is effectively the product of Figs. 3a–3d according to Eq. (1). However, small contributions from laser-sheet attenuation, saturation, and the camera gating time, together amounting to <15% signal variation, have also been included in the final image.

It is interesting to note that the fluorescence intensity stays within a factor of 5 everywhere in the image, despite the quenching rate increasing by a factor of 40 across the shock (and consequently the fluorescence yield decreases by a factor of 18). The signal decrease caused by the collisional quenching is mostly offset by fivefold increases in the NO number density and Boltzmann fraction as shown in Figs. 3 and 4. Note that in Fig. 4 each curve is a plot of the parameter magnitude for a horizontal cross section taken 6 mm above the wedge.

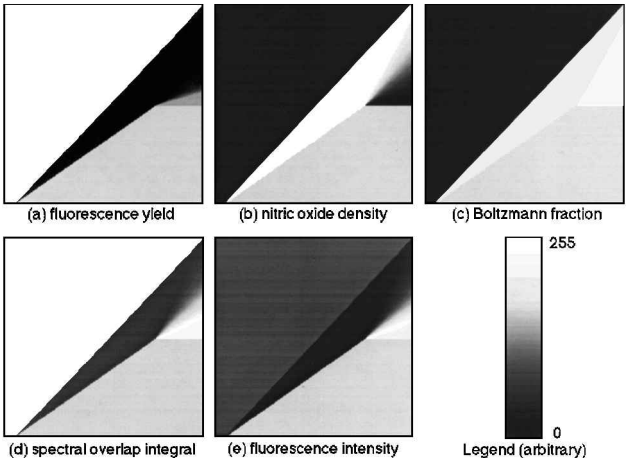

Fig. 3 Typical spatial variations of calculated parameters contributing to a CFI-PLIF image for excitation of the $^{R}R_{22}(26.5)$ line of NO.

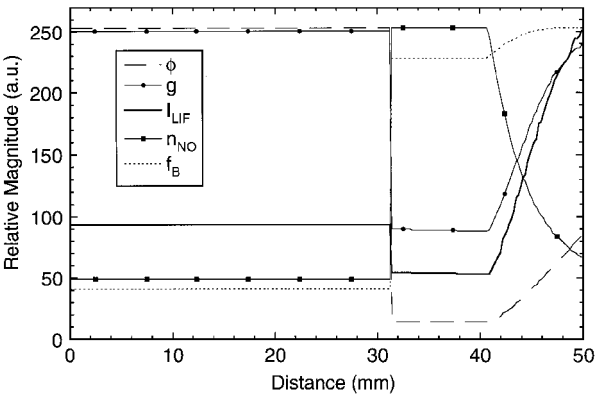

Fig. 4 Plot of one row of calculated parameters contributing to a CFI-PLIF image for the conditions shown in Fig. 3.

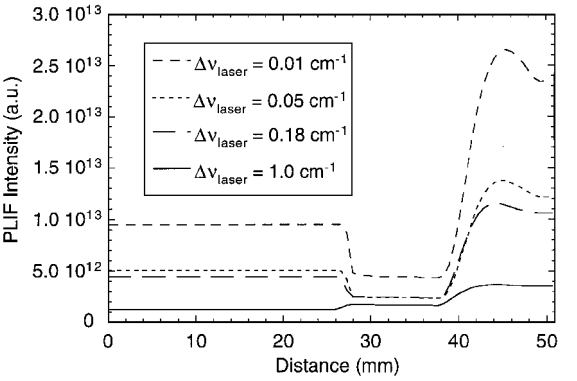

Fig. 5 Calculated PLIF intensity for similar conditions as Fig. 3 but with four different values of the laser linewidth.

The spectral overlap integral g varies by less than a factor of three in the computation. Thus, its contribution to the signal is not a dominating factor in this experiment. However, because g is strongly dependent on the laser's frequency and linewidth, it can dominate the appearance of an image under some circumstances. For example, Fig. 5 shows that if the linewidth of the laser varies by a factor of 10 or 100 (which can be realized in the laboratory by using intracavity etalons and/or injection seeding), the fluorescence intensity changes appreciably. As the laser's linewidth increases, the magnitude of the fluorescence intensity decreases because the laser is much broader than the transition and thus the spectral overlap decreases. A second important trend shown in Fig. 5 is that the signal becomes more uniform throughout the image as the laser linewidth increases. This is because Doppler and collisional shifts are not large enough to move the absorbing frequency outside the laser profile when the laser linewidth is large. In Fig. 5, each curve is a plot of the predicted PLIF intensity for a horizontal cross section taken 4 mm above the wedge.

Computation of fluorescence intensities for a variety of laser linewidths is an excellent example of the utility of this CFI-PLIF method. Based on this computation, one might choose to use a larger laser linewidth in an imaging experiment to ensure that there will be ample signal intensities throughout the imaged region. This could be very important, for example, in the case of 2-line PLIF thermometry experiments.[12] Conversely, if desired, one can use a narrow-linewidth laser to exaggerate the signal variation due to Doppler or pressure shifts. This might be particularly useful in PLIF velocimetry.

According to the computation, the low-intensity laser sheet used in this experiment only saturates the transition slightly in the freestream ($I/I_{sat} = 0.15$) and negligibly in the postshock region ($I/I_{sat} = 0.02$). Furthermore, the fractional beam attenuation is negligible in the freestream (0.004 per cm) and only slightly noticeable in the postshock region (0.03 per cm).

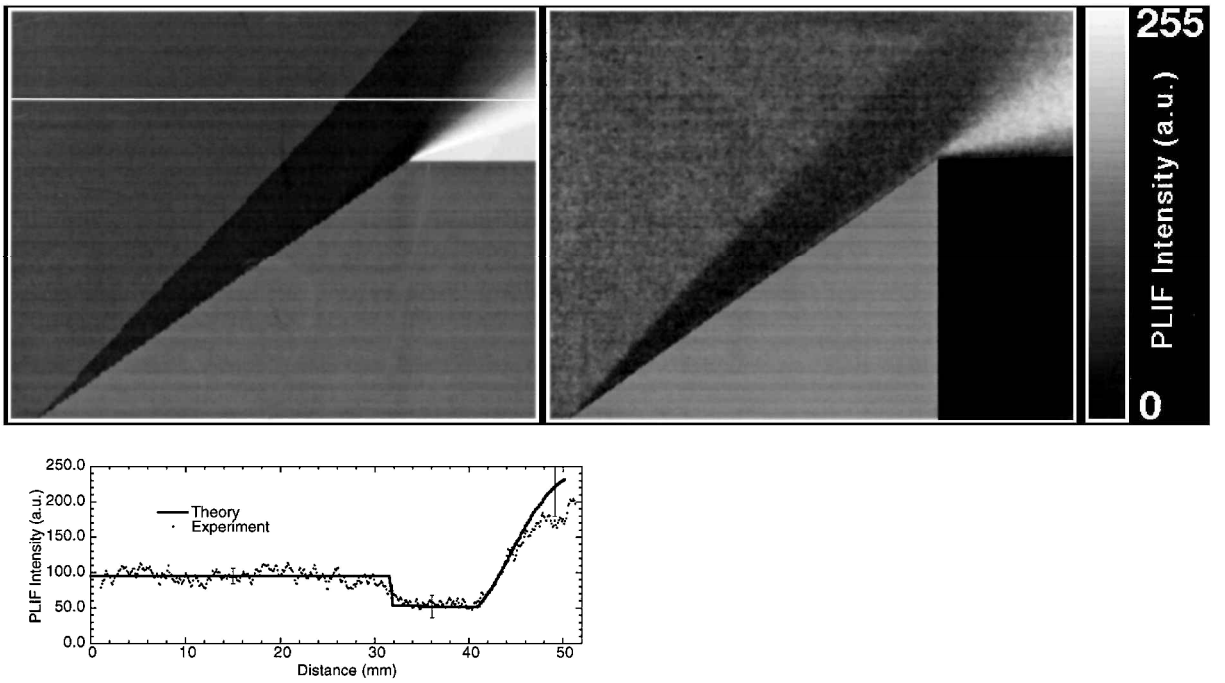

Fig. 6 Comparison between theoretical (top left) and experimental (top right) wedge flow images.

B. Wedge Results

Figure 6 shows the comparison between the calculated and experimental PLIF images for the wedge flow. The flow is from left to right, and the laser sheet enters from the top of the image. The bottom of the image corresponds to the centerline of the flow. The graph represents a horizontal slice through both images above the shoulder of the wedge as indicated by the horizontal line on the theory image. The error bars show the estimated uncertainty in the CFI-PLIF theory, based on $\Delta U'$ (see Sec. VI). The imaged region is 50×39 mm. The experimental image in Fig. 6 is an average of four single-shot PLIF images of the ${}^{R}R_{22}(26.5)$ line of NO. These images were averaged to reduce shot nose and also to reduce the uncertainty in signal intensity due to laser mode structure as described earlier.

The theoretical PLIF images agree well with the experiment. The predicted shock angle of 46.5 ± 0.7 deg agrees extremely well with the shock angle measured from the images: 46.5 ± 0.5 deg. Because shock angle is a relatively strong function of γ, this agreement supports that our supposition that the vibrational modes are frozen. [The vibrational relaxation length behind the shock is greater than 10 cm (Ref. 9), whereas our entire imaged region is half that size.]

The intensities of the calculated PLIF images also show close agreement with experiment. The calculated PLIF image was arbitrarily scaled to match the experimental signal intensity in the freestream. In both experiment and theory, the signal drops by about a factor of two across the shock. Both images show the signal rapidly rising in the expansion region; however, the maximum signal in the expansion region for the experimental image is lower than the calculation. This discrepancy may be because the large PLIF intensity saturated the 8-bit ICCD camera on three of the four images used to produce the experimental image. The one unsaturated image showed a signal increase from freestream to expansion of nearly a factor of three: similar to the calculation. In the future, we will avoid detector saturation by using an ICCD camera with a larger dynamic range.

C. Hemisphere Results

Figure 7 shows the comparison between a calculated image and a single-shot experimental PLIF image for the hemisphere flow. The flow is from left to right, and the laser sheet enters from the top of the image. The bottom of the image corresponds to the centerline of the flow. The experimental image is from a single tunnel run. The left graph represents a horizontal slice through both images just above the hemisphere as indicated by the horizontal white line on the theoretical image. The right graph is a diagonal cut from the bottom left corner to top right corner as indicated on the theoretical image. The imaged region is 39×39 mm. As discussed in Sec. II.A.3, the calculated images exclude the effects of vibrational nonequilibrium, which are appreciable both in the freestream and in the region of the postshock flow away from the stagnation point.

For the transition excited $[{}^{P}P_{11}(35.5)]$, the PLIF intensity rises dramatically across the shock and then remains roughly constant as the gas accelerates from zero velocity at the stagnation point to supersonic speeds farther downstream.

Although the shock shapes in the two images are similar, a closer comparison between experimental and theoretical shock-standoff distances points out a significant discrepancy. The measured shock-standoff distance divided by the radius of the hemisphere is approximately 0.14, whereas that value determined from the computation is 0.11. This discrepancy can be attributed entirely to the incorrect assumption of vibrational equilibrium that is inherent in the computation. In fact, these two shock-standoff distances correspond closely to those predicted for chemically frozen flow in the limits of vibrationally frozen ($\gamma = 1.4$) and vibrationally equilibrated ($\gamma = 1.29$) diatomic flows, respectively.[21] Recall that the CFD code used earlier to compute the wedge flow assumed the flow was vibrationally frozen, resulting in excellent agreement between the shock angles in experiment and theory.

Figure 7 shows that the intensities of the calculated PLIF image also show reasonable agreement with the experiment, especially considering that properties such as the pressure vary by up to a factor of 50 in the image. The calculated PLIF image was arbitrarily scaled to match the experimental signal intensity in the postshock stagnation region. According to this scaling, the theory slightly overpredicts the PLIF intensity in the freestream. This could also be caused, again, by the assumption of vibrational equilibrium in the computation: the artificially high freestream temperature (by 120 K) incorrectly predicts a larger signal for this high-rotational-quantum-number transition. However, the more likely reason for this discrepancy is that the fluctuations in the laser mode structure result in 25% uncertainties in the PLIF intensity in the freestream, as described earlier.

In the shock layer, the agreement between experiment and theory is reasonably good, but discrepancies occur as the flow continues to expand around the hemisphere. Based on the large uncertainties in both the experiment and the calculation (see Sec. VI), it is difficult to say whether the observed discrepancies are caused by improper modeling of the fluid dynamics or the fluorescence or because this image is based on a single tunnel run. Nonetheless, the CFI-PLIF predicts the same trends as seen in the experiment.

Table 1 Flow parameters and normalized sensitivities in each region of the wedge flow, computed for the conditions of the experiment

Parameter	Units	Region 1	S_i	Region 2	S_i	Region 3	S_i	Region 4	S_i
T	K	440	2.23	3080	−1.65	2290	−1.49	1470	−0.90
P	Pa	4500	0.63	163000	−0.46	57400	−0.21	12100	0.29
V_y	m/s	0	n.a.	1330	0.08	848	0.15	0	n.a.
χ_{NO}		0.0111	0.64	0.0111	0.69	0.0111	0.61	0.0111	0.59
I	W/cm^2	24.7	0.87	23.9	0.98	23.1	0.97	22.2	0.92
ν_{laser}	cm^{-1}	−0.061	1.04	0.20	−0.91	0.089	−0.68	−0.060	0.80
$\Delta\nu_{laser}$	cm^{-1}	0.18	−0.37	0.18	0.03	0.18	−0.17	0.18	−0.27
Q ($\times 10^6$)	1/s	3.89	−0.44	152	−0.96	50.1	−0.90	9.70	−0.67

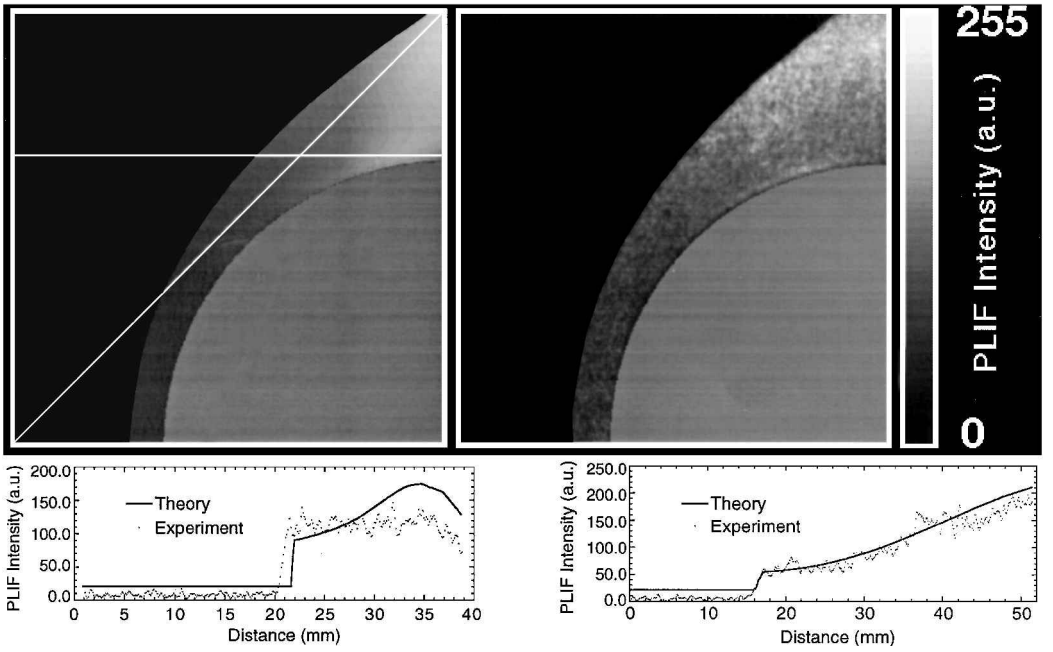

Fig. 7 Comparison between theoretical (top left) and experimental (top right) hemisphere flow images.

V. Sensitivity Study

We have computed the sensitivity of the CFI-PLIF intensity to the most important input parameters: both fluid mechanical and spectroscopic. These sensitivities are used next to determine the uncertainty in the CFI-PLIF intensity due to uncertainty in the various input parameters to the code. This sensitivity study can also provide insight toward developing new diagnostic capabilities.

The normalized sensitivity S_i of the CFI-PLIF intensity to a parameter P_i is

$$S_i \equiv \frac{\partial I_{\mathrm{LIF}}}{\partial P_i} \Big/ \frac{I_{\mathrm{LIF}}}{P_i} \tag{6}$$

$$S_i \approx \frac{\Delta I_{\mathrm{LIF}}/I_{\mathrm{LIF}}}{\Delta P_i/P_i} \tag{7}$$

where i is an index indicating a specific input parameter. It is normalized so that the sensitivity indicates the relationship between fractional changes in the input parameter and fractional changes in the CFI-PLIF intensity. For example, a sensitivity of unity indicates that a 1% change in the parameter results in a 1% change in the CFI-PLIF intensity. The sensitivity was computed by running the CFI-PLIF code for slightly different input parameters and using the results to evaluate Eq. (7).

When varying one parameter influences others substantially, we determine the sensitivity by expanding out the differential. For example, small changes in the flow velocity cause large changes in the temperature and pressure throughout the flowfield. We then use the following equation to isolate the changes in CFI-PLIF intensity caused by the change in individual parameters:

$$\frac{\Delta I_{\mathrm{LIF}}}{I_{\mathrm{LIF}}} = \sum_i S_i \frac{\Delta P_i}{P_i} \tag{8}$$

In general, there is one such equation for each input parameter. Thus, a system of N equations and N unknowns can be solved in each flow region to determine the various sensitivities based on N different runs of the CFI-PLIF code, each with unique input parameters.

We have performed this sensitivity analysis for the case of flow over the wedge (see Sec. II.A.2). We evaluated the sensitivity at one point in each of the four regions in Fig. 1. Points 1–4 are located precisely where their respective numerals are shown in Fig. 1. Table 1 shows the results of the sensitivity analysis computed for the same conditions as Fig. 6.

Several interesting conclusions can be drawn from these results. First, a review of Table 1 shows that CFI-PLIF is most sensitive to changes in temperature. For the rotational quantum number J, chosen for the computation ($J = 26.5$), the sensitivity was a positive number greater than unity in the cold freestream and a negative number less than -1 in the hot postshock region. In other words, a 1% increase in the temperature would cause a 2.23% increase in PLIF intensity in the freestream, but would cause a 1.65% decrease in intensity in the postshock region. The sensitivity of the CFI-PLIF to temperature is mainly caused by the exponential temperature dependence in the Boltzmann fraction f_{Bi}. This computation confirms the widely known fact that, depending on the selected J, PLIF is very sensitive to temperature and is, thus, a sensitive method for performing thermometry.

Compared to the temperature, the CFI-PLIF intensity is much less sensitive to the pressure. In this computation, the NO mole fraction is constant, and so increasing the pressure increases the NO number density, which increases the PLIF intensity. However, increasing the pressure also increases the quenching rate, which decreases the PLIF intensity. These two effects offset each other resulting in a weak dependence on pressure resulting mainly from the overlap integral and because Q and A are comparable in the fluorescence yield term.

For the orientation of the laser sheet with respect to the flow direction in this experiment, the CFI-PLIF intensity is insensitive to the flow velocity. In region 2, for example, the temperature and pressure are very high, and so the absorption is very broad. This results in a low sensitivity to Doppler shifts in the absorption spectrum. If the laser frequency was shifted approximately one-half of the transition linewidth, the sensitivity of the CFI-PLIF intensity to velocity would be maximized, which would be ideal for velocimetry.

The CFI-PLIF intensity shows a weak dependence on the mole fraction of NO. An increase in mole fraction results in both an increase in NO number density and an increase in quenching because NO–NO self-quenching is one of the dominant quenching mechanisms in this flow. These two effects partially cancel each other, resulting in sensitivity less than unity. There is little laser-beam attenuation caused by NO absorption at these conditions, so that laser beam attenuation has little influence on the sensitivity.

The laser intensity in this experiment was chosen so that $I \ll I_{\text{sat}}$. Thus, the CFI-PLIF intensity shows a near-unity sensitivity to the laser intensity.

The sensitivity to changes in the laser frequency was computed differently than the other parameters because tiny fractional changes in the absolute laser frequency result in massive changes in PLIF intensity. Instead, the sensitivity has been computed for small changes in laser frequency as a fraction of the laser's linewidth. Further, the value of ν_{laser} shown in Table 1 is the frequency shift between the laser frequency and the peak of the pressure and Doppler shifted absorption spectrum. The computed sensitivities range from 1.04 to −0.91 depending on where the pressure and Doppler shifts have moved the absorption peak relative to the laser tuning.

The PLIF intensity is comparatively insensitive to variations in the laser linewidth. The computed sensitivities are consistent with the results of Fig. 4, which shows that increasing the laser linewidth decreases the signal in regions 1, 3, and 4, whereas it has little effect on the signal in the postshock region, due to the large pressure and Doppler broadening there.

Finally, we determined the sensitivity to the quenching rate by adjusting the quenching cross section for NO–NO self-quenching (the dominant quencher in the flow) by a small amount and then using Eq. (8) to compute the resulting sensitivity. In all cases, increases in quenching cause decreases in CFI-PLIF intensity. This effect is most severe, however, in the postshock region where $Q \gg A$, and so the fluorescence yield term is proportional to A/Q. In the freestream, Q and A are comparable, and variations in quench rate have less influence on the PLIF intensity.

VI. Uncertainty Analysis

We have determined the uncertainty in our CFI-PLIF computations based on the uncertainties in the various inputs and the sensitivities to these inputs. We computed the overall fractional uncertainty ΔU

$$\Delta U^2 = \sum_i (S_i \Delta U_i)^2 \tag{9}$$

where ΔU_i is the fractional uncertainty in the parameter i. Table 2 shows the result of the uncertainty analysis for the same four regions of the flow. The uncertainties shown are expressed as a fraction of the parameter and are based on computations of the flow conditions considering the uncertainty in the measured input parameters (such as shock speed and shock tube fill pressure) combined with knowledge of various random and systematic errors present in the system.

The computed uncertainties is rather large: in the range of ±27–40%. The largest contributions to this uncertainty are from 1) inaccurately measuring the laser intensity, 2) large uncertainties in the quenching cross sections taken from the literature, and 3) a large uncertainty in the NO mole fraction because of a low level of confidence in the chemical and vibrational nonequilibrium models used to predict the freestream composition. Note that uncertainties in the freestream temperature are amplified by the large sensitivity of the CFI-PLIF signal to temperature. On the other hand, averaging the results of five experiments reduced the uncertainty associated with the absolute tuning of the laser frequency.

Because comparisons between experiment and theory in Sec. IV have been arbitrarily scaled by a constant for best fit, we have effectively removed uncertainties associated with parameters that scale the image as a whole, i.e., parameters that have similar magnitudes and sensitivities in all of the flow regions. Thus, in our comparisons, we have effectively avoided uncertainties associated with the laser intensity and NO mole fraction and to a lesser extent quenching. By excluding the uncertainties from the laser intensity and the NO mole fraction, we obtain smaller estimates of the uncertainty $\Delta U'$, also shown in Table 2, that are more relevant to the comparison of experimental and computational PLIF images shown in this paper.

The large uncertainties associated with the CFI-PLIF images limits the use of this method for directly validating CFD codes. Typically, one would hope to compare hypersonic CFD codes with experimental data that are accurate to ±10% or better. However, CFI-PLIF can still be useful for designing experiments. It can still be used to predict trends and to test out various detection strategies. Furthermore, when no other comparison between experiment and theory can be made, CFI-PLIF offers a reasonable method for comparison.

Two sources of uncertainty present in the experiments have not been included in the CFI-PLIF computation and, thus, are not included in the uncertainty analysis. These are image shot noise and the effect of shot-to-shot variations in the laser mode structure. The signal variations shown in the graph of Fig. 6 are typical of the shot noise in the present experiment. Typically, the shot noise amounted to a 6% uncertainty in the experiments.

Pulse-to-pulse variations in the laser mode structure influence the LIF intensity through the spectral overlap integral g_i. We have theoretically estimated the uncertainty in the overlap integral from a simple model for the laser mode fluctuations.[22] For the conditions of the four flow regions described earlier, we computed at least 100 simulated laser profiles and computed the standard deviation of the resulting overlap integral. For a single image, the predicted uncertainties (equal to the standard deviation) ranged from 10% of the signal intensity in the freestream where the transition linewidth is smaller than the laser linewidth to 2% of the signal intensity in the postshock region where the transition linewidth is broad compared to the laser. Averaging four images in the present experiment reduced these uncertainties by a factor of 1.7. Thus, shot noise and laser mode fluctuations caused comparable uncertainties in the experiment. However, the experimental uncertainty was smaller than the uncertainty in the theoretical images.

Table 2 Computed fractional uncertainties for the wedge flow

	Region 1		Region 2		Region 3		Region 4	
Parameter	ΔU_i	$S_i \Delta U_i$	ΔU_i	$S_i \Delta U_i$	ΔU_i	$S_i \Delta U_i$	ΔU_i	$S_i \Delta U_i$
T	0.034	0.076	0.034	−0.056	0.034	−0.051	0.034	−0.031
P	0.044	0.028	0.044	−0.021	0.044	−0.009	0.044	0.013
V_y	n.a.	n.a.	0.010	0.001	0.010	0.002	n.a.	n.a.
χ_{NO}	0.150	0.096	0.150	0.104	0.150	0.092	0.150	0.089
I	0.250	0.218	0.250	0.245	0.250	0.244	0.250	0.230
ν_{laser}	0.050	0.052	0.050	−0.046	0.050	−0.034	0.050	0.040
$\Delta\nu_{\text{laser}}$	0.056	−0.021	0.056	0.001	0.056	−0.009	0.056	−0.015
Q	0.150	−0.066	0.300	−0.288	0.200	−0.181	0.150	−0.101
ΔU	0.27		0.40		0.32		0.27	
$\Delta U'$	0.12		0.30		0.19		0.11	

Several precautions can be taken in future experiments to decrease the uncertainties in the computed images. First, the laser intensity should be measured more accurately with a wavemeter on each run. Second, we can determine the NO mole fraction spectroscopically to achieve a higher accuracy. Third, we can change the gas composition of the flow so that quenchers with better known quenching cross sections dominate. In the current experiments, N_2, which has a poorly understood quench cross section above 2000 K (Ref. 6), is the dominant quencher in region 2. O_2 and NO have better understood quenching cross sections, and so increasing the amount of these species in the test gas would decrease the uncertainty associated with quenching. Fourth, averaging more images would reduce the uncertainties associated with laser mode fluctuations. All of these methods would improve the accuracy of the CFI-PLIF computations.

VII. Conclusions

We have presented a theoretical model for predicting PLIF images and have compared this model with two different hypersonic shock-layer measurements. The theoretical model uses CFD codes to produce maps of temperature, pressure, velocity, and species concentrations. The frequency, linewidth, and energy of the exciting laser are used with the results of the CFD to compute fluorescence images. The model determines the contributions to collisional quenching from all of the molecules in the flow. It includes computation of the Boltzmann fraction for the molecular transitions excited and the spectral overlap between the laser and the excited transition(s). The model also addresses several effects that were not dominant in this experiment: laser-sheet attenuation, saturation of the molecular transition, and the finite intensifier gating time. The model could be improved by including a more rigorous treatment of effects related to laser-mode fluctuations, the finite duration of the laser pulse, and population transfer between the various energy modes in the molecular system.

The relative intensities of experimental and theoretical PLIF images for the wedge experiments compare well. Agreement for the flow over the hemisphere was not as good, though the agreement was within the uncertainties of the calculations and measurements. Although the comparisons shown offer considerable support for the PLIF model, further comparisons with a CFD code that includes vibrational nonequilibrium would more fully validate the method. Furthermore, several aspects of the experiment could be performed differently to decrease the uncertainties in the resulting images. Several physical effects included in the model, such as the laser-sheet attenuation and the excitation of overlapping transitions, have not been throughly tested in this experiment. These will be addressed in future experiments.

Sensitivity and uncertainty analyses have also been performed. The uncertainty analysis suggests that, in its present form, CFI-PLIF should be used cautiously for directly validating CFD codes. However, it can be used reliably for predicting trends while designing PLIF experiments.

Acknowledgments

This work was funded by the Australian Research Council. The authors would like to thank Paul Walsh at the Australian National University for his technical assistance, and Peter Mere from the Australian National University and M. D. DiRosa and P. H. Paul at Sandia National Laboratories Livermore, California, for their support.

References

[1]Boyce, R. R., Morton, J. W., Houwing, A. F. P., Mundt, C., and Bone, D. J., "CFD Validation Using Multiple Interferometric Views of Three Dimensional Shock Layer Flows over a Blunt Body," AIAA Paper 94-0282, Jan. 1994.

[2]Houwing, A. F. P., Kamel, M., Morris, C., Thurber, M., Wehe, S., Boyce, R. R., and Hanson, R. K., "PLIF Imaging and Thermometry of NO/N2 Shock Layer Flows in an Expansion Tube," AIAA Paper 96-0537, Jan. 1996.

[3]Palmer, J. L., McMillin, B. K., and Hanson, R. K., "Planar Laser-Induced Fluorescence Imaging of Velocity and Temperature in Shock Tunnel Freejet Flow," AIAA Paper 92-0762, Jan. 1992.

[4]Palma, P. C., McIntyre, T. J., and Houwing, A. F. P., "PLIF Imaging of Nitric Oxide in High-Enthalpy Flows," *Proceedings of the 20th International Symposium on Shock Waves*, edited by B. Sturtevant, J. E. Shepherd, and H. G. Hornung, World Scientific, Singapore, 1996, pp. 1617–1622.

[5]Wollenhaupt, M., Rosenhauer, M., Muller, T., Beck, W. H., and Scheer, M., "Spatially and Spectrally Resolved Laser-Induced Fluorescence Measurements in the HEG," *Proceedings of the 20th International Symposium on Shock Waves*, edited by B. Sturtevant, J. E. Shepherd, and H. G. Hornung, World Scientific, Singapore, 1996, pp. 281–286.

[6]Paul, P. H., Gray, J. A., Durant, J. L., Jr., and Thoman, J. W., Jr., "Collisional Quenching Corrections for Laser-Induced Fluorescence Measurements of NO $A^2\Sigma^+$," *AIAA Journal*, Vol. 32, No. 8, 1994, pp. 1670–1675.

[7]Ruyten, W. M., Williams, W. D., and Heltsley, F. L., "Computational Flow Imaging for Planar Laser-Induced Fluorescence Applications (CFI-PLIF)," AIAA Paper 94-2621, June 1994.

[8]Vardavas, I. M., "Modeling Reactive Gas Flows Within Shock Tunnels," *Australian Journal of Physics*, Vol. 37, No. 2, 1984, pp. 157–177.

[9]Vincenti, W. G., and Kruger, J. C., Jr., *Introduction to Physical Gas Dynamics*, Kreiger, Malabar, FL, 1965, Chap. 7.

[10]Liepmann, H. W., and Roshko, A., *Elements of Gasdynamics*, Wiley, New York, 1957, Chap. 12.

[11]Mundt, C., "Calculation of Hypersonic, Viscous, Nonequilibrium Flows Around Re-Entry Bodies Using a Coupled Boundary Layer/Euler Method," AIAA Paper 92-2856, July 1992.

[12]Hanson, R. K., Seitzman, J. M., and Paul, P. H., "Planar Laser-Fluorescence Imaging of Combustion Gases," *Applied Physics B*, Vol. 50, June 1990, pp. 441–454.

[13]Siegman, A. E., *Lasers*, Univ. Science Books, Mill Valley, CA, 1986, p. 293.

[14]Danehy, P. M., Friedman-Hill, E. J., Lucht, R. P., and Farrow, R. L., "The Effects of Collisional Quenching on Degenerate Four-Wave Mixing," *Applied Physics B*, Vol. 57, 1993, pp. 243–248.

[15]Eckbreth, A. C., *Laser Diagnostics for Combustion Temperature and Species*, 2nd ed., Gordon and Breach Amsterdam, 1996, Chap. 7.

[16]Boyd, R. W., *Nonlinear Optics*, Academic, San Diego, CA, 1992, Chap. 5.

[17]Stalker, R. J., "A Study of the Free-Piston Shock Tunnel," *AIAA Journal*, Vol. 5, No. 12, 1967, pp. 2160–2165.

[18]McIntosh, M. K., "Computer Program for the Numerical Calculation of Frozen Equilibrium Conditions in Shock Tunnels," Dept. of Physics, Australian National Univ., Canberra, Australia, Sept. 1968.

[19]Palma, P. C., Danehy, P. M., and Houwing, A. F. P., "Non-Intrusive Thermometry in Shock Layers Using Multi-Line Fluorescence Imaging," *Proceedings of the 21st International Symposium on Shock Waves*, edited by A. F. P. Houwing, Panther Publishing, Fyshwick, Australia, 1998, pp. 447–452.

[20]Seitzman, J. M., Hanson, R. K., DeBarber, P. A., and Hess, C. F., "Application of Quantitative Two-Line OH PLIF for Temporally Resolved Planar Thermometry in Reacting Flows," *Applied Optics*, Vol. 33, No. 18, 1994, pp. 4000–4012.

[21]Hornung, H. G., "Non-Equilibrium Dissociating Nitrogen Flows over Spheres and Circular Cylinders," *Journal of Fluid Mechanics*, Vol. 53, 1972, pp. 149–176.

[22]McMillin, B. K., "Instantaneous Two-Line PLIF Temperature Imaging of Nitric Oxide in Supersonic Mixing and Combustion Flowfields," Ph.D. Dissertation, Mechanical Engineering Dept., Stanford Univ., Stanford, CA, May 1993.

R. P. Lucht
Associate Editor